



# Physicochemical properties of phenyltrifluoroborate-based room temperature ionic liquids



Kazuki Iwasaki <sup>a</sup>, Kazuki Yoshii <sup>a</sup>, Tetsuya Tsuda <sup>a,\*</sup>, Susumu Kuwabata <sup>a,b,\*\*</sup>

<sup>a</sup> Department of Applied Chemistry, Graduate School of Engineering, Osaka University, 2-1 Yamada-oka, Suita, Osaka 565-0871, Japan

<sup>b</sup> Department of Energy and Environment, Research Institute of Electrochemical Energy, National Institute of Advanced Industrial Science and Technology, 1-8-31 Midorigaoka, Ikeda, Osaka 563-8577, Japan

## ARTICLE INFO

### Article history:

Received 17 August 2017

Received in revised form 15 September 2017

Accepted 17 September 2017

Available online 20 September 2017

### Keywords:

Room temperature ionic liquid

Phenyltrifluoroborate

Fluoroanion

Aromatic structure

Physicochemical properties

## ABSTRACT

Novel room temperature ionic liquids (RTILs) were synthesized using phenyltrifluoroborate ( $[\text{PhBF}_3]^-$ ), which is the simplest aryltrifluoroborate structure. The  $[\text{PhBF}_3]^-$ -based RTILs showed desirable transport properties, i.e., viscosity and ionic conductivity, and the anion has a rigid and bulky aromatic ring. The properties of 1-butyl-3-methylimidazolium phenyltrifluoroborate ( $[\text{C}_4\text{mim}][\text{PhBF}_3]$ ) are comparable to those of 1-butyl-3-methylimidazolium tetrafluoroborate ( $[\text{C}_4\text{mim}][\text{BF}_4]$ ). The molecular volume of the RTILs, which was estimated using the appropriate quantum chemical calculations, highly correlated with the transport properties. The cation volume is an important factor that can control the physicochemical properties in this RTIL system. In addition, the basic skeleton structure of the cation determined the electrochemical window.

© 2017 Elsevier B.V. All rights reserved.

## 1. Introduction

Room temperature ionic liquids (RTILs), liquid salts that contain only a cation and an anion at room temperature, are a subset of molten salts that possess unique features, such as negligible vapor pressures, incombustibility, wide electrochemical windows (EWs), and relatively high ionic conductivities [1,2]. The features of RTILs, except for the handling temperatures, are very similar to those of molten salts, which are very useful anhydrous solvents for high-temperature electrochemical technologies, including the Hall-Héroult process and molten carbonate fuel cell systems. These appealing features are why many different applications have been proposed for RTILs, e.g., next generation energy devices [3–8], recyclable and nonvolatile organic synthesis processes [9, 10], high-performance lubricants [11,12], and functional liquid materials for vacuum technologies [13–17]. The number of fundamental science articles related to RTILs has increased in recent years because scientists can readily design and synthesize the ionic species in RTILs but not in conventional solvents. In the past several decades, numerous cations and anions have been used to prepare various functional RTILs. The basic skeletons for typical cations include imidazolium, pyridinium, pyrrolidinium, piperidinium, quaternary ammonium, sulfonium, and

phosphonium. Their common side chains include straight alkyl, aminoalkyl, hydroxyalkyl, alkoxyalkyl, and other groups, and  $\text{AlCl}_4^-$ ,  $\text{BF}_4^-$ ,  $\text{PF}_6^-$ ,  $\text{CF}_3\text{SO}_3^-$ ,  $\text{N}(\text{SO}_2\text{CF}_3)_2^-$ ,  $\text{N}(\text{CN})_2^-$ , and  $(\text{FH})_n\text{F}^-$  ( $1 \leq n \leq 3$ ) have been widely used as the anion component [18,19]. The physicochemical properties of RTILs strongly depend on the cation and anion species combination [20–26]. For example, 1-butyl-1-methylpyrrolidinium bis(trifluoromethylsulfonyl)amide ( $[\text{C}_4\text{mpyr}][\text{N}(\text{SO}_2\text{CF}_3)_2]$ ) has a viscosity of 76 mPa·s, but when the cation component is changed to 1-ethyl-3-methylimidazolium ( $[\text{C}_2\text{mim}]^+$ ), the viscosity significantly decreases to 35 mPa·s [27,28]. Changing the anion component also results in changes in the properties of the RTIL. Unfortunately, the design and synthesis of novel anion species is difficult compared to that of the cations that have been synthesized using a simple nucleophilic substitution reaction [29] because the anion synthetic process is not well-established and laborious.

Very recently, we successfully synthesized nearly 40 types of aryltrifluoroborate anions ( $[\text{ArBF}_3]^-$ ) and reported the unique physicochemical properties of alkali metal salts with  $[\text{ArBF}_3]^-$  [30]. Potassium and cesium salts with  $[\text{ArBF}_3]^-$  can be easily prepared on a large scale using commercially available reagents [31].  $[\text{ArBF}_3]^-$  is an analog of tetrafluoroborate ( $[\text{BF}_4]^-$ ), which is a typical RTIL anion first reported by Wilkes and Zaworotko [32], and in  $[\text{ArBF}_3]^-$ , one fluorine in  $[\text{BF}_4]^-$  is replaced with a designable aromatic ring. Because of the ring, organic salts with  $[\text{ArBF}_3]^-$  are likely to have favorable physicochemical properties because of the decreased interionic interaction energy between the anions and cations due to the lower surface charge density on the anions as a result of adding an electron-withdrawing phenyl group [27,33–

\* Corresponding author.

\*\* Correspondence to: Department of Applied Chemistry, Graduate School of Engineering, Osaka University, 2-1 Yamada-oka, Suita, Osaka 565-0871, Japan.

E-mail addresses: [tsuda@chem.eng.osaka-u.ac.jp](mailto:tsuda@chem.eng.osaka-u.ac.jp) (T. Tsuda), [kuwabata@chem.eng.osaka-u.ac.jp](mailto:kuwabata@chem.eng.osaka-u.ac.jp) (S. Kuwabata).

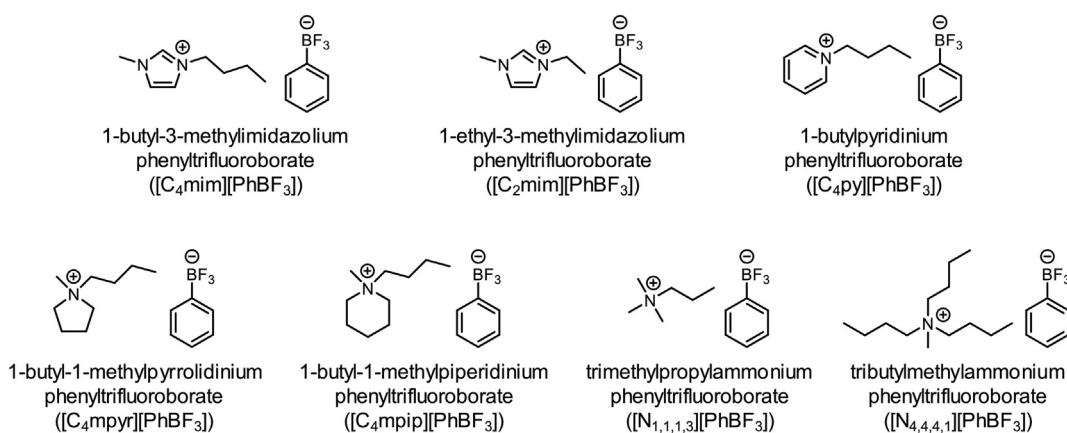


Fig. 1. Chemical structures of [PhBF<sub>3</sub>]<sup>−</sup>-based RTILs with different organic cations and their abbreviations.

40]. In this study, we attempted to produce undiscovered RTILs by combining different onium cations, e.g., imidazolium, pyridinium, pyrrolidinium, piperidinium, and quaternary ammonium, with the phenyltrifluoroborate ([PhBF<sub>3</sub>]<sup>−</sup>) anion, which has the simplest structure among the [ArBF<sub>3</sub>]<sup>−</sup> anions. The physicochemical properties of the resulting [PhBF<sub>3</sub>]<sup>−</sup>-based salts were examined. The factors controlling their properties were explored via systematic data gathering.

## 2. Experimental section

Potassium phenyltrifluoroborate (K[PhBF<sub>3</sub>]) was synthesized using phenylboronic acid (PhB(OH)<sub>2</sub>) (Wako Pure Chemical Industries, Ltd.), potassium fluoride (KF) (Wako Pure Chemical Industries, Ltd.), and L-tartaric acid (Wako Pure Chemical Industries, Ltd.) in the following procedure [31]. An aqueous solution of KF (200 mmol, 20 mL) was added to a solution of PhB(OH)<sub>2</sub> (50 mmol) in acetonitrile (200 mL), and the mixture was stirred for 15 min at ambient temperature. L-Tartaric acid (2.05 equiv.) dissolved in tetrahydrofuran (THF) (100 mL) was slowly added to the mixture, and then, a white by-product immediately precipitated. The reaction mixture was vigorously stirred for 1 h at ambient temperature and filtered to remove the precipitate. The resultant filtrate was concentrated in vacuo, and the crude potassium salt was obtained as a solid. The crude product was purified by recrystallization to obtain pure K[PhBF<sub>3</sub>]. The obtained salt was dried at 353 K under vacuum for 1 h. The final product was confirmed by nuclear magnetic resonance (NMR) spectroscopy, mass spectrometry, and elemental analysis.

Seven kinds of onium salts, 1-ethyl-3-methylimidazolium chloride ([C<sub>2</sub>mim]Cl) (Tokyo Chemical Industry Co., Ltd.), 1-butyl-3-methylimidazolium chloride ([C<sub>4</sub>mim]Cl) (Kanto Chemical Co., Inc.), 1-butylpyridinium chloride ([C<sub>4</sub>py]Cl) (Tokyo Chemical Industry Co., Ltd.), 1-butyl-1-methylpyrrolidinium chloride ([C<sub>4</sub>mpyr]Cl) (Sigma-Aldrich, Inc.), 1-butyl-1-methylpiperidinium chloride ([C<sub>4</sub>mpip]Cl) (Tokyo Chemical Industry Co., Ltd.), trimethylpropylammonium bromide ([N<sub>1,1,1,3</sub>]Br) (Tokyo Chemical Industry Co., Ltd.), and tributylmethylammonium chloride ([N<sub>4,4,4,1</sub>]Cl) (Sigma-Aldrich, Inc.) were used as the cationic species for the preparation of the [PhBF<sub>3</sub>]<sup>−</sup>-based organic salts. K[PhBF<sub>3</sub>] was prepared via the previously mentioned protocol and was used as the anion source. The synthesis of the [PhBF<sub>3</sub>]<sup>−</sup>-based organic salts was performed using the metathesis protocol explained below. K[PhBF<sub>3</sub>] (40 mmol) was added to a solution of an onium halide (40 mmol) in acetonitrile (60 mL), and the mixture was stirred for 1 h at ambient temperature. After the reaction, the mixture was filtered to remove the precipitated by-product, KCl or KBr, and the filtrate was condensed under vacuum. The crude product was extracted by CH<sub>2</sub>Cl<sub>2</sub> and rinsed with ultrapure water several times to remove the unreacted halides and by-product. The organic layer was concentrated in vacuo. The resultant onium phenyltrifluoroborate was dried at 373 K under vacuum for 12 h. The final product was confirmed

by NMR spectroscopy, mass spectrometry, and elemental analysis. 1-Butyl-3-methylimidazolium tetrafluoroborate ([C<sub>4</sub>mim][BF<sub>4</sub>]) was purchased from Kanto Chemical Co. and used for comparison. It was thoroughly vacuum dried for 24 h before use to remove any residual water.

Thermogravimetric (TG) analyses were performed using a Bruker TG-DTA2000SA instrument. Samples were placed on an open aluminum pan and heated from room temperature to 773 K at a rate of 5 K·min<sup>−1</sup> under flowing dry nitrogen gas. The thermal degradation temperature was determined from the 5 wt% loss point of the TG curve. Differential scanning calorimetry (DSC) was conducted using a Bruker DSC3100SA instrument. The samples were sealed in an aluminum pan with an aluminum top. The sealed pan was heated and cooled at a rate of 5 K·min<sup>−1</sup>. The glass-transition temperature and melting point were obtained from the DSC curve of the second heating process. These values were estimated using the tangential intersection method near the temperature at which a phase transformation occurred. These two instruments were controlled with a Bruker MTC1000SA workstation utilizing the Bruker WS003 software. All the specimens for these measurements were prepared in an argon gas-filled glove box (Vacuum Atmospheres Co., Omni-Lab, O<sub>2</sub> and H<sub>2</sub>O < 1 ppm).

Density measurements were conducted using a Kyoto Electronics Manufacturing DA-640 resonant frequency oscillation density/specific gravity meter in the range of 298–353 K. The viscosity was measured

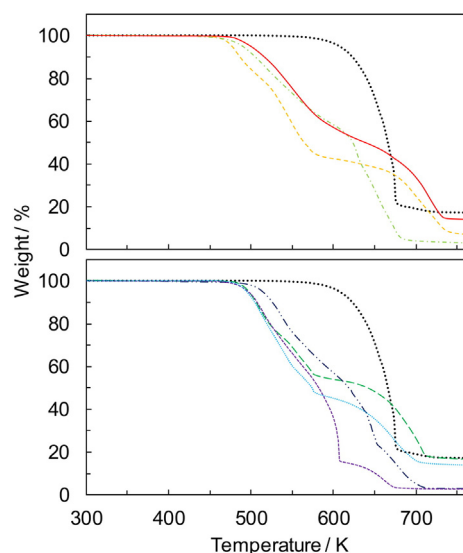


Fig. 2. Results of the TG analysis for (•••) [C<sub>4</sub>mim][BF<sub>4</sub>], (—) [C<sub>4</sub>mim][PhBF<sub>3</sub>], (---) [C<sub>2</sub>mim][PhBF<sub>3</sub>], (— · —) [C<sub>4</sub>py][PhBF<sub>3</sub>], (· · · ·) [C<sub>4</sub>mpyr][PhBF<sub>3</sub>], (— · · ·) [C<sub>4</sub>mpip][PhBF<sub>3</sub>], (•••) [N<sub>1,1,1,3</sub>][PhBF<sub>3</sub>], and (— · —) [N<sub>4,4,4,1</sub>][PhBF<sub>3</sub>]. The measurements were conducted at a rate of 5 K·min<sup>−1</sup>.

**Table 1**  
Physicochemical properties of  $[\text{PhBF}_3]^-$ -based RTILs and salts.

RTILs and salt	FW <sup>a</sup>	$T_g^b$ /K	$T_m^c$ /K	$T_d^d$ /K	$d^e$ /g·cm <sup>-3</sup>	$\eta^f$ /mPa·s	$\sigma^g$ /mS·cm <sup>-1</sup>	$\Lambda^h$ /S·cm <sup>2</sup> ·mol <sup>-1</sup>	$V_{\text{cation}}^i$ /nm <sup>3</sup>	$V_{\text{anion}}^j$ /nm <sup>3</sup>
$[\text{C}_4\text{mim}][\text{BF}_4]$	226	190	—	611	1.201	101	4.21	0.795	0.207	0.072
$[\text{C}_4\text{mim}][\text{PhBF}_3]$	284	209	—	492	1.145	115	2.42	0.602	0.207	0.164
$[\text{C}_2\text{mim}][\text{PhBF}_3]$	255	210	—	477	1.192	60	7.09	1.54	0.160	0.164
$[\text{C}_4\text{py}][\text{PhBF}_3]$	281	224	—	490	1.151	131	2.20	0.539	0.203	0.164
$[\text{C}_4\text{mpyr}][\text{PhBF}_3]$	287	208	—	497	1.114	241	1.44	0.371	0.211	0.164
$[\text{C}_4\text{mpip}][\text{PhBF}_3]$	301	228	—	514	1.108	1150	0.328	0.0895	0.231	0.164
$[\text{N}_{1,1,1,3}][\text{PhBF}_3]$	274	—	350	495	—	—	—	—	0.160	0.164
$[\text{N}_{4,4,4,1}][\text{PhBF}_3]$	345	227	—	496	1.028	1870	0.112	0.0377	0.319	0.164

The ionic volume was calculated with the Gaussian 09 program using a B3LYP/6-31G+(d) level calculation.

<sup>a</sup> Formula weight.

<sup>b</sup> Glass-transition temperature.

<sup>c</sup> Melting point.

<sup>d</sup> Thermal degradation temperature at 5 wt% loss.

<sup>e</sup> Density at 298 K.

<sup>f</sup> Viscosity at 298 K.

<sup>g</sup> Ionic conductivity at 303 K.

<sup>h</sup> Equivalent conductivity at 303 K.

<sup>i</sup> Volume of the cation.

<sup>j</sup> Volume of the anion.

using a Kyoto Electronics Manufacturing EMS-1000 electromagnetically spinning viscometer in the range of 298–353 K. Ionic conductivity measurements were performed using a Horiba DS-51 digital conductivity meter in the range of 303–353 K with a glass conductivity cell after the cell was calibrated with a 0.1 M KCl aqueous solution. The electrochemical measurements were conducted with an IVIUM Technologies CompactStat portable electrochemical analyzer. All electrochemical experiments were performed in a three-electrode cell. The working electrode was a glassy carbon disk (1.6 mm in diameter), which was

polished with an alumina suspension (0.06  $\mu\text{m}$  in diameter) prior to use. A platinum wire (0.5 mm in diameter) was used as the counter electrode, and the reference electrode was constructed by placing a 1.0 mm diameter Ag wire into a 6 mm diameter Vycor® glass tube filled with a  $[\text{C}_4\text{mim}][\text{N}(\text{SO}_2\text{CF}_3)_2]$  RTIL containing 0.05 M  $\text{Ag}[\text{N}(\text{SO}_2\text{CF}_3)_2]$ . All the measurements, except the viscosity, were performed in an argon-filled glove box. The viscosity measurements were performed using the special airtight cells for the electromagnetically spinning viscometer. The Gaussian 09 program [41] was used for the molecular orbital calculations. We used the basis sets implemented in the Gaussian program. All the ion structures used in this study were optimized at the HF/6-311G(d,p) level. The ionic volumes of the cations and anions were calculated at the B3LYP/6-31G+(d) level [20]. We determined the ionic volume using the average value from 10 calculations.

### 3. Results and discussion

#### 3.1. General characteristics

The chemical structures of the organic salts prepared in this study are summarized in Fig. 1 with their abbreviations. We successfully synthesized seven types of  $[\text{PhBF}_3]^-$ -based organic salts. All the salts,

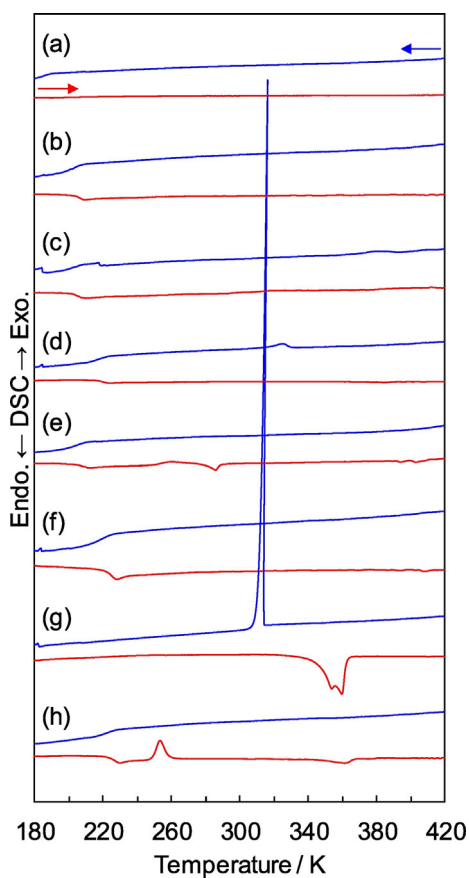


**Fig. 3.** DSC curves of (a)  $[\text{C}_4\text{mim}][\text{BF}_4]$ , (b)  $[\text{C}_4\text{mim}][\text{PhBF}_3]$ , (c)  $[\text{C}_2\text{mim}][\text{PhBF}_3]$ , (d)  $[\text{C}_4\text{py}][\text{PhBF}_3]$ , (e)  $[\text{C}_4\text{mpyr}][\text{PhBF}_3]$ , (f)  $[\text{C}_4\text{mpip}][\text{PhBF}_3]$ , (g)  $[\text{N}_{1,1,1,3}][\text{PhBF}_3]$ , and (h)  $[\text{N}_{4,4,4,1}][\text{PhBF}_3]$ . The measurements were conducted at a rate of 5 K·min<sup>-1</sup>.

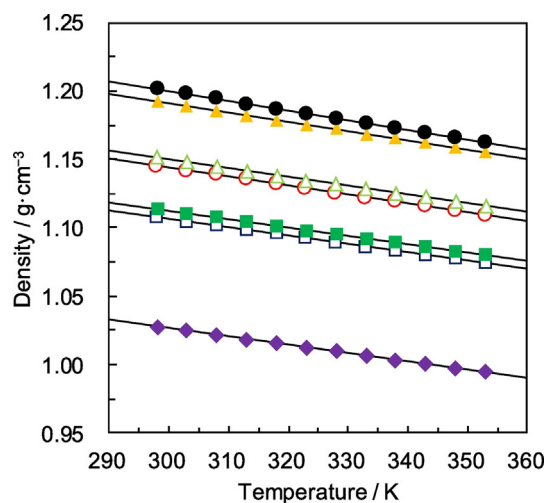


**Fig. 4.** Temperature dependence of the density for (●)  $[\text{C}_4\text{mim}][\text{BF}_4]$ , (○)  $[\text{C}_4\text{mim}][\text{PhBF}_3]$ , (▲)  $[\text{C}_2\text{mim}][\text{PhBF}_3]$ , (△)  $[\text{C}_4\text{py}][\text{PhBF}_3]$ , (■)  $[\text{C}_4\text{mpyr}][\text{PhBF}_3]$ , (□)  $[\text{C}_4\text{mpip}][\text{PhBF}_3]$ , and (◆)  $[\text{N}_{4,4,4,1}][\text{PhBF}_3]$ . The solid lines depicted on each plot are the approximate lines calculated using the least-square method.

**Table 2**  
Fitted parameters for the density of the RTILs with various cations.

RTILs	$a/\text{g}\cdot\text{cm}^{-3}$	$b \times 10^4/\text{g}\cdot\text{cm}^{-3}\cdot\text{K}^{-1}$	$ R $
[C <sub>4</sub> mim][BF <sub>4</sub> ]	1.413	−7.113	>0.9999
[C <sub>4</sub> mim][PhBF <sub>3</sub> ]	1.339	−6.510	>0.9999
[C <sub>2</sub> mim][PhBF <sub>3</sub> ]	1.392	−6.711	>0.9999
[C <sub>4</sub> py][PhBF <sub>3</sub> ]	1.340	−6.362	>0.9999
[C <sub>4</sub> mpyr][PhBF <sub>3</sub> ]	1.297	−6.136	>0.9999
[C <sub>4</sub> mPIP][PhBF <sub>3</sub> ]	1.288	−6.048	>0.9999
[N <sub>4,4,4,1</sub> ][PhBF <sub>3</sub> ]	1.207	−6.020	>0.9999

except [N<sub>1,1,1,3</sub>][PhBF<sub>3</sub>], were liquid salts at room temperature. K[PhBF<sub>3</sub>] has a melting point of 568 K [30], but the cation exchange of K<sup>+</sup> for the organic cations caused a sudden drop in the melting point due to the larger cation size and the asymmetric structure of the organic cations. The resulting organic salts were stable in air without any undesirable reactions with oxygen and moisture even though they were moderately hygroscopic. All the salts had a lower water miscibility than the salts with [BF<sub>4</sub>]<sup>−</sup>, and the hydrophobic phenyl group in [PhBF<sub>3</sub>]<sup>−</sup> causes this characteristic.

### 3.2. Thermal behavior

The TG analysis results for the [PhBF<sub>3</sub>]<sup>−</sup>-based salts are shown in Fig. 2 along with the results for [C<sub>4</sub>mim][BF<sub>4</sub>] as a comparison. The thermal degradation temperatures determined at a 5 wt% loss are given in Table 1. All the salts exhibited clear weight losses at temperatures in the range from 477 to 514 K, and their thermal stabilities were inferior to that of [C<sub>4</sub>mim][BF<sub>4</sub>]. This result is attributed to the [PhBF<sub>3</sub>]<sup>−</sup> anion containing a B–C bond because the bond dissociation energy of the B–C bond (92 kcal·mol<sup>−1</sup>) is smaller than that of the B–F bond (181 kcal·mol<sup>−1</sup>) in [BF<sub>4</sub>]<sup>−</sup> [42]. The TG curves also indicated that the thermal degradation reaction proceeds via multiple steps, whereas [C<sub>4</sub>mim][BF<sub>4</sub>] showed a simple one-step curve. As expected, the weight losses observed for the first one or two steps were very close to the wt% of the [PhBF<sub>3</sub>]<sup>−</sup> in the original RTILs, e.g., 51 wt% in [C<sub>4</sub>mim][PhBF<sub>3</sub>] and 56 wt% in [C<sub>2</sub>mim][PhBF<sub>3</sub>]. The DSC curves for the same RTILs are given in Fig. 3. Almost all the salts showed a glass-transition temperature ( $T_g$ ) at 208–228 K, but they did not show significant crystallization or melting behaviors, except for [N<sub>1,1,1,3</sub>][PhBF<sub>3</sub>], which showed a sharp exothermic peak in the cooling process at ca. 313 K and a noticeable endothermic peak in the heating process at 353 K without any glass-transition behavior (Fig. 3g). In the case of [C<sub>4</sub>mpyr][PhBF<sub>3</sub>] and [N<sub>4,4,4,1</sub>][PhBF<sub>3</sub>], small crystallization and melting behaviors were observed (Fig. 3e and h). These behaviors are induced by the very slow dynamics derived from the unique properties of RTILs [43,44].

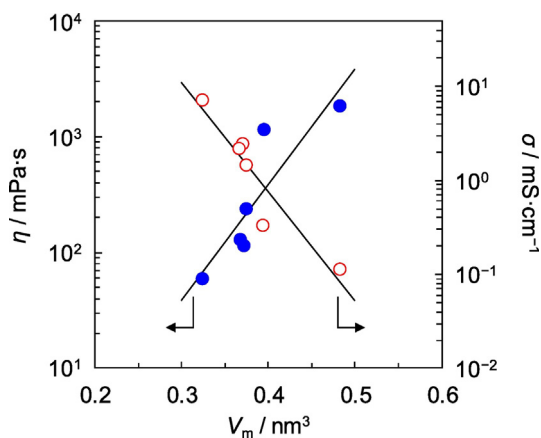


**Fig. 5.** Correlation between the (●) ionic pair volume and viscosity at 298 K and the (○) ionic pair volume and ionic conductivity at 303 K. The original data are given in Fig. 4 and Table 1.

Unfortunately, certain information about such phase transitions could only be obtained using a specially manufactured DSC at this time [45].

### 3.3. Physicochemical properties

The density data for the [PhBF<sub>3</sub>]<sup>−</sup>-based RTILs at 298 K are given in Table 1 along with other physicochemical properties. The temperature dependence of the density ( $d$ ) of the [PhBF<sub>3</sub>]<sup>−</sup>-based RTILs is shown in Fig. 4. The solid lines depicted in the figure are straight lines that were calculated using the least-squares method. In general, density can be represented as a function of absolute temperature by the following equation:

$$d = a + bT \quad (1)$$

where  $a$  is the density at 0 K ( $\text{g}\cdot\text{cm}^{-3}$ ),  $b$  is a volume expansion coefficient ( $\text{g}\cdot\text{cm}^{-3}\cdot\text{K}^{-1}$ ), and  $T$  is the absolute temperature (K). The results fitted by the least-squares method are summarized in Table 2. The correlation coefficient ( $|R|$ ) indicates the precision of the fitting. The densities of the [PhBF<sub>3</sub>]<sup>−</sup>-based liquid salts were 1.028–1.192  $\text{g}\cdot\text{cm}^{-3}$  at 298 K (Table 1), and these values were closely related to the cationic volume. The ascending order of the cation volume based on the B3LYP/6-31G+(d) level calculations using the Gaussian 09 program [41] is [C<sub>2</sub>mim]<sup>+</sup> (0.160 nm<sup>3</sup>) < [C<sub>4</sub>py]<sup>+</sup> (0.203 nm<sup>3</sup>) < [C<sub>4</sub>mim]<sup>+</sup> (0.207 nm<sup>3</sup>) < [C<sub>4</sub>mpyr]<sup>+</sup> (0.211 nm<sup>3</sup>) < [C<sub>4</sub>mPIP]<sup>+</sup> (0.231 nm<sup>3</sup>) < [N<sub>4,4,4,1</sub>]<sup>+</sup> (0.319 nm<sup>3</sup>), and this order coincides with the descending order of the density. Several research groups have concluded that the molecular volumes of RTILs are related to some of their physicochemical parameters, e.g., density, viscosity, melting point, and dielectric constant [46–48]. As we will discuss later, a similar relationship was also observed in our RTILs.

The [PhBF<sub>3</sub>]<sup>−</sup>-based RTILs showed viscosities ( $\eta$ ) ranging from 60 to 1870 mPa·s at 298 K and ionic conductivities ( $\sigma$ ) ranging from 0.112 to 7.09 mS·cm<sup>−1</sup> at 303 K (Table 1). The RTILs with aromatic cations, i.e., [C<sub>4</sub>mim]<sup>+</sup>, [C<sub>2</sub>mim]<sup>+</sup>, and [C<sub>4</sub>py]<sup>+</sup>, had favorable transport properties. Most RTILs with a  $\pi$ -conjugated cation show a similar tendency [49, 50]. The compact volume of aromatic cations, not the liquid structure of RTILs, contributes to the transport properties, as shown in Fig. 5, and this indicates that the molecular volume is related to the viscosity and conductivity. The following equations proposed by Krossing et al. were used to fit the data [48].

$$\eta = a_1 e^{b_1 V_m} \quad (2)$$

$$\sigma = a_2 e^{-b_2 V_m} \quad (3)$$

where  $a_1$  (mPa·s) and  $a_2$  (mS·cm<sup>−1</sup>) are the empirical pre-exponential factors,  $b_1$  (nm<sup>−3</sup>) and  $b_2$  (nm<sup>−3</sup>) are the empirical constants, and  $V_m$  (nm<sup>3</sup>) is the molecular volume of each organic cation and the [PhBF<sub>3</sub>]<sup>−</sup> anion in the RTILs. Their volumes were estimated using quantum chemical calculations, and the data are summarized in Table 1. The fitting parameters for Eqs. (2) and (3) are  $a_1 = 4.00 \times 10^{-2}$ ,  $b_1 = 22.9$ ,  $a_2 = 3.48 \times 10^4$ , and  $b_2 = 26.8$ . Interestingly, even though [C<sub>4</sub>mPIP][PhBF<sub>3</sub>] has some deviations, the plots for all the RTILs agree well with the equations, suggesting that the cation volume is an important factor in the [PhBF<sub>3</sub>]<sup>−</sup>-based RTIL system. The obtained slopes,  $b_1$  and  $b_2$ , were larger than those for the other anions, e.g., [BF<sub>4</sub>]<sup>−</sup>, [N(CN)<sub>2</sub>]<sup>−</sup>, and [N(SO<sub>2</sub>CF<sub>3</sub>)<sub>2</sub>]<sup>−</sup> [48]. The values for  $b_1$  are related to the strength of the intermolecular interactions in the RTILs, and the same applies to  $b_2$ . In the [PhBF<sub>3</sub>]<sup>−</sup>-based RTILs, a stronger interaction was observed compared to the RTILs with other anions, which was contrary to our expectation that the interionic interaction energy would decrease due to the electron-withdrawing phenyl group on the anion. The unexpected behavior could be due to the extra interaction induced by the dynamic contact resistance between the organic cation and the bulky phenyl group on [PhBF<sub>3</sub>]<sup>−</sup>.

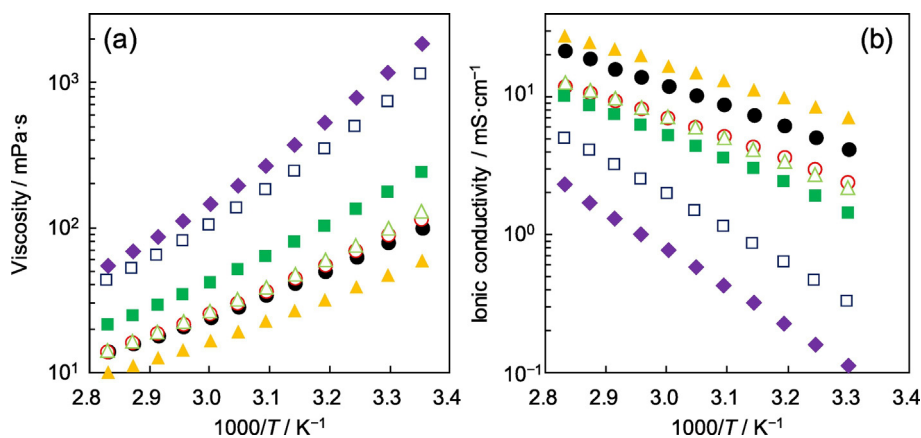


Fig. 6. Arrhenius plots of the (a) viscosities and (b) ionic conductivities for (●) [C<sub>4</sub>mim][BF<sub>4</sub>], (○) [C<sub>4</sub>mim][PhBF<sub>3</sub>], (▲) [C<sub>2</sub>mim][PhBF<sub>3</sub>], (△) [C<sub>4</sub>py][PhBF<sub>3</sub>], (■) [C<sub>4</sub>mpyr][PhBF<sub>3</sub>], (□) [C<sub>4</sub>mpip][PhBF<sub>3</sub>], and (◆) [N<sub>4,4,4,1</sub>][PhBF<sub>3</sub>].

Arrhenius plots of the viscosity and ionic conductivity for the RTILs with [PhBF<sub>3</sub>]<sup>−</sup> are shown in Fig. 6a and b, respectively. Each plot shows gentle curves, and the curves are common for glass-forming RTILs. In general, the activation energies of the transport properties, viscosity and ionic conductivity can be discussed using Arrhenius plots. However, using the plots to discuss the temperature dependence of glass-forming liquids is difficult because of the complex system generated by the super-Arrhenius behavior [51]. In this case, the Vogel–Tammann–Fulcher (VTF) equation, as expressed below, can be used to fit the transport properties. Eqs. (4) and (5) show the VTF equation for the viscosity and the equivalent ionic conductivity ( $\Lambda$ ·cm<sup>2</sup>·mol<sup>−1</sup>), respectively [52,53].

$$\ln \eta = \frac{k_{\eta}}{T - T_0} + \frac{1}{2} \ln T - \ln A_{\eta} \quad (4)$$

$$- \ln \Lambda = \frac{k_{\Lambda}}{T - T_0} + \frac{1}{2} \ln T - \ln A_{\Lambda} \quad (5)$$

where  $k_{\eta}$  (K) is a constant related to the Arrhenius activation energy for the viscous behavior,  $k_{\Lambda}$  (K) is a constant related to the conduction behavior,  $T_0$  (K) is an ideal glass-transition temperature,  $A_{\eta}$  is a scaling factor for the viscosity, and  $A_{\Lambda}$  is a scaling factor for the equivalent ionic conductivity. The experimental results for the specific ionic conductivity can be converted to the equivalent conductivity using the following equation.

$$\Lambda = \sigma M / d \quad (6)$$

where  $M$  is the formula weight (g·mol<sup>−1</sup>) and  $d$  is the density (g·cm<sup>−3</sup>). The fitted parameters obtained from Eqs. (4) and (5) are summarized in Table 3. The temperature-dependent activation energies for the viscosity ( $E_{a,\eta}$ ) and the equivalent conductivity ( $E_{a,\Lambda}$ ) are given by

the following equations, which involve the partial differentiation of Eqs. (4) and (5), respectively, with respect to temperature [52,53].

$$E_{a,\eta} = -RT^2 \left( \frac{\partial \ln \eta}{\partial T} \right) = \frac{Rk_{\eta}T^2}{(T - T_0)^2} - \frac{RT}{2} \quad (7)$$

$$E_{a,\Lambda} = RT^2 \left( \frac{\partial \ln \Lambda}{\partial T} \right) = \frac{Rk_{\Lambda}T^2}{(T - T_0)^2} - \frac{RT}{2} \quad (8)$$

The resulting plots of  $E_{a,\eta}$  and  $E_{a,\Lambda}$  versus the absolute temperature are shown in Fig. 7. The ionic transport activation energies of the RTILs strongly depended on the cation volume and temperature. The RTILs with larger cations had higher activation energies, and this suggests that the cation structure has a large effect on the activation energy, which directly influences the transport properties. The activation energies decreased as the temperature increased, and almost all the  $E_{a,\eta}$  values were higher than the  $E_{a,\Lambda}$  values at each temperature [20,22,54]. Given that the differential capacitance measured via an AC impedance technique is different from the capacitance estimated using the static method because of the ultra-slow response to the electric double layer formation [55], the observed differences between the  $E_{a,\eta}$  and  $E_{a,\Lambda}$  values may be due to the AC impedance method used to perform the ionic conductivity measurement.

The Walden plot method and pulsed-field-gradient spin-echo (PGSE) NMR [56] spectroscopy are often used to estimate the dissociation degree of RTILs, i.e., the ionicity. Here, to investigate the ionicity of the [PhBF<sub>3</sub>]<sup>−</sup>-based RTILs at each temperature, we evaluated the degree of the ionic dissociation using the Walden plot method that requires data on the equivalent ionic conductivity and the reciprocal of the viscosity [20,22,57]. In Fig. 8, the Walden plots of the [PhBF<sub>3</sub>]<sup>−</sup>-based RTILs are shown, and the plots of [C<sub>4</sub>mim][BF<sub>4</sub>] are included for comparison. The diagonal line in the figure is an ideal line for a 1 M KCl aqueous

Table 3  
Fitted parameters for the VTF equations for the viscosity and equivalent conductivity of the [PhBF<sub>3</sub>]<sup>−</sup>-based RTILs.

RTILs	Derived from the viscosity				Derived from the equivalent conductivity			
	$T_0$ /K	$k_{\eta}$ /K	$\ln A_{\eta}$	R	$T_0$ /K	$k_{\Lambda}$ /K	$\ln A_{\Lambda}$	R
[C <sub>4</sub> mim][BF <sub>4</sub> ]	171	$8.71 \times 10^2$	5.08	0.9999	148	$2.70 \times 10^3$	13.2	0.9999
[C <sub>4</sub> mim][PhBF <sub>3</sub> ]	168	$9.61 \times 10^2$	5.48	0.9999	152	$1.04 \times 10^3$	9.21	0.9999
[C <sub>2</sub> mim][PhBF <sub>3</sub> ]	166	$8.45 \times 10^2$	5.15	0.9999	132	$1.41 \times 10^3$	10.6	0.9999
[C <sub>4</sub> py][PhBF <sub>3</sub> ]	176	$9.03 \times 10^2$	5.37	0.9999	148	$1.19 \times 10^3$	9.90	0.9999
[C <sub>4</sub> mpyr][PhBF <sub>3</sub> ]	176	$9.89 \times 10^2$	5.46	0.9999	162	$1.09 \times 10^3$	9.62	0.9999
[C <sub>4</sub> mpip][PhBF <sub>3</sub> ]	195	$1.00 \times 10^3$	5.53	0.9999	180	$2.78 \times 10^3$	14.5	0.9999
[N <sub>4,4,4,1</sub> ][PhBF <sub>3</sub> ]	182	$1.31 \times 10^3$	6.59	0.9999	178	$4.14 \times 10^3$	17.2	0.9999

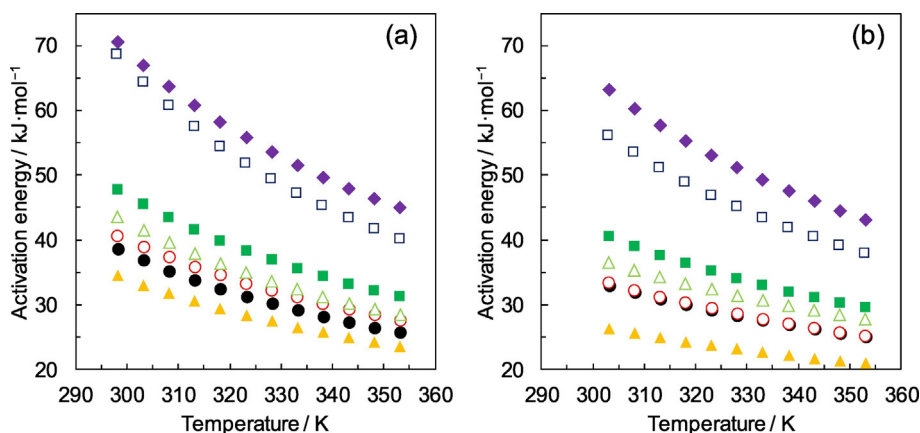


**Fig. 7.** Temperature-dependent activation energies for the (a) viscosity and (b) equivalent conductivity for (●) [C<sub>4</sub>mim][BF<sub>4</sub>], (○) [C<sub>4</sub>mim][PhBF<sub>3</sub>], (▲) [C<sub>2</sub>mim][PhBF<sub>3</sub>], (△) [C<sub>4</sub>py][PhBF<sub>3</sub>], (■) [C<sub>4</sub>mpyr][PhBF<sub>3</sub>], (□) [C<sub>4</sub>mpip][PhBF<sub>3</sub>], and (◆) [N<sub>4,4,4,1</sub>][PhBF<sub>3</sub>].

solution that is regarded as an ideal dissociation state. If there are partially associated ion pairs in RTILs, the plots deviate from the ideal line, and the degree of ionic dissociation can be visually estimated based on the deviation. Interestingly, the plots of most of the [PhBF<sub>3</sub>]<sup>−</sup>-based RTILs and [C<sub>4</sub>mim][BF<sub>4</sub>] were close to the ideal line. The small gaps between the ideal line and the plots imply that the RTILs have favorable dissociation degrees. In terms of the ionicity, the introduction of the phenyl group to BF<sub>3</sub> did not have a large influence.

### 3.4. Electrochemical analyses

The electrochemical stability, which is generally called the EW [58], of the RTILs with [PhBF<sub>3</sub>]<sup>−</sup> was examined via linear sweep voltammetry. The obtained voltammograms are shown in Fig. 9. Each scan was initiated from the open circuit potential, and all the cathodic limiting potentials ( $E_{\text{cathodic}}$ ), the anodic limiting potentials ( $E_{\text{anodic}}$ ), and the EWs ( $\text{EW} = E_{\text{anodic}} - E_{\text{cathodic}}$ ) were estimated from Fig. 9. The electrochemical data are summarized in Table 4. The ascending order of the RTIL EWs is [C<sub>4</sub>py][PhBF<sub>3</sub>] (2.42 V) < [C<sub>2</sub>mim][PhBF<sub>3</sub>] (3.71 V) < [C<sub>4</sub>mim][PhBF<sub>3</sub>] (3.78 V) < [N<sub>4,4,4,1</sub>][PhBF<sub>3</sub>] (4.40 V) < [C<sub>4</sub>mpip][PhBF<sub>3</sub>] (4.55 V) < [C<sub>4</sub>mpyr][PhBF<sub>3</sub>] (4.67 V). The RTILs with a quaternary ammonium cation, which is known to be more electrochemically stable than aromatic cations, showed wider EWs. Typically, the cathodic and anodic limiting reactions in RTILs are the decompositions of the cation and anion, respectively [27,36,38]. The anodic limiting potentials of the RTILs with [PhBF<sub>3</sub>]<sup>−</sup> had relatively similar values of 0.584–0.804 V

(vs. Ag(I)/Ag), but the potentials were substantially lower than those with [BF<sub>4</sub>]<sup>−</sup> (ca. 1.65 V). This was probably due to the oxidizable electron-rich phenyl group in [PhBF<sub>3</sub>]<sup>−</sup>. In contrast, the cathodic stabilities differed based on the cation structure. The quaternary ammonium cations, [C<sub>4</sub>mpyr]<sup>+</sup>, [C<sub>4</sub>mpip]<sup>+</sup>, and [N<sub>4,4,4,1</sub>]<sup>+</sup>, had a higher stability than that of the other aromatic cations. [C<sub>4</sub>py]<sup>+</sup> had the lowest cathodic stability, and the stability difference from [C<sub>2</sub>mim]<sup>+</sup> was ca. 1.1 V. This is an acceptable potential gap considering the reported values observed in [C<sub>2</sub>mim][AlCl<sub>4</sub>] and [C<sub>4</sub>py][AlCl<sub>4</sub>] [59].

### 4. Conclusions

We successfully synthesized six novel RTILs and one organic salt with [PhBF<sub>3</sub>]<sup>−</sup>. Their thermal stabilities are moderate and do not exceed that of the [BF<sub>4</sub>]<sup>−</sup>-based RTILs due to the decomposition of [PhBF<sub>3</sub>]<sup>−</sup>, which has a thermally unstable B–C bond. However, the other physicochemical properties of the [PhBF<sub>3</sub>]<sup>−</sup>-based RTILs were basically favorable even though [PhBF<sub>3</sub>]<sup>−</sup> is a relatively rigid and large anion compared to the typical anion components in RTILs. Introducing the phenyl group to the BF<sub>3</sub> structure was not problematic. In RTIL systems, the cationic species as well as the anionic ones has a major effect on the physicochemical properties. Several design criteria for RTIL systems were successfully obtained. The fundamental findings reported in this article will be useful for creating currently unknown functional RTILs.

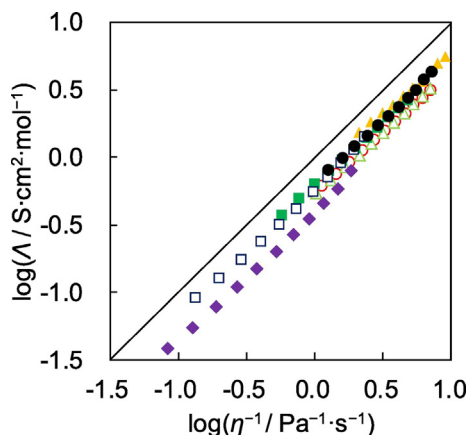


**Fig. 8.** Walden plots for (●) [C<sub>4</sub>mim][BF<sub>4</sub>], (○) [C<sub>4</sub>mim][PhBF<sub>3</sub>], (▲) [C<sub>2</sub>mim][PhBF<sub>3</sub>], (△) [C<sub>4</sub>py][PhBF<sub>3</sub>], (■) [C<sub>4</sub>mpyr][PhBF<sub>3</sub>], (□) [C<sub>4</sub>mpip][PhBF<sub>3</sub>], and (◆) [N<sub>4,4,4,1</sub>][PhBF<sub>3</sub>]. The solid line in the figure is an ideal line constructed from the data for a 1 M KCl aqueous solution.

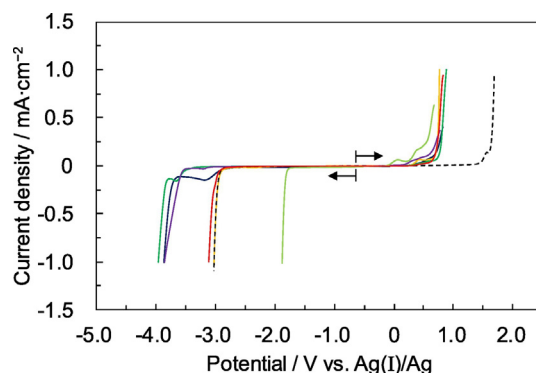


**Fig. 9.** Linear sweep voltammograms recorded at a glassy carbon electrode in (---) [C<sub>4</sub>mim][BF<sub>4</sub>], (—) [C<sub>4</sub>mim][PhBF<sub>3</sub>], (—) [C<sub>2</sub>mim][PhBF<sub>3</sub>], (—) [C<sub>4</sub>py][PhBF<sub>3</sub>], (—) [C<sub>4</sub>mpyr][PhBF<sub>3</sub>], (—) [C<sub>4</sub>mpip][PhBF<sub>3</sub>], and (—) [N<sub>4,4,4,1</sub>][PhBF<sub>3</sub>] at 298 K. The scan rate was 10 mV·s<sup>−1</sup>.

**Table 4**  
Cathodic and anodic limits and electrochemical windows for the [PhBF<sub>3</sub>]<sup>−</sup>-based RTILs.

RTILs	$E_{\text{cathodic}}^a/V$ vs. Ag(l)/Ag	$E_{\text{anodic}}^b/V$ vs. Ag(l)/Ag	EW <sup>c</sup> /V
[C <sub>4</sub> mim][BF <sub>4</sub> ]	−2.99	1.65	4.64
[C <sub>4</sub> mim][PhBF <sub>3</sub> ]	−3.04	0.745	3.78
[C <sub>2</sub> mim][PhBF <sub>3</sub> ]	−2.97	0.739	3.71
[C <sub>4</sub> py][PhBF <sub>3</sub> ]	−1.84	0.584	2.42
[C <sub>4</sub> mpyr][PhBF <sub>3</sub> ]	−3.86	0.804	4.67
[C <sub>4</sub> mpip][PhBF <sub>3</sub> ]	−3.76	0.787	4.55
[N <sub>4,4,4,1</sub> ][PhBF <sub>3</sub> ]	−3.66	0.735	4.40

<sup>a</sup> Cathodic limiting potential at the cut-off current density of  $-0.3 \text{ mA} \cdot \text{cm}^{-2}$ .

<sup>b</sup> Anodic limiting potential at the cut-off current density of  $0.3 \text{ mA} \cdot \text{cm}^{-2}$ .

<sup>c</sup> Electrochemical window;  $\text{EW} = E_{\text{anodic}} - E_{\text{cathodic}}$ .

## Acknowledgments

This research was partially supported by JSPS KAKENHI Grant Numbers JP15H03591, JP15K13287, JP15H02202, and JP16K14539 and by the Advanced Low Carbon Technology Research and Development Program (ALCA) for Specially Promoted Research for Innovative Next Generation Batteries (SPRING), Japan Science and Technology Agency (JST).

## Appendix A. Supplementary data

Supplementary data to this article can be found online at <https://doi.org/10.1016/j.molliq.2017.09.067>.

## References

- T. Tsuda, C.L. Hussey, Electrochemistry of room-temperature ionic liquids and melts, in: R.E. White (Ed.), *Modern Aspects of Electrochemistry*, Springer Science + Business Media, New York 2009, pp. 63–174.
- Y. Ito, T. Nohira, Non-conventional electrolytes for electrochemical applications, *Electrochim. Acta* 45 (2000) 2611–2622.
- T. Sato, G. Masuda, K. Takagi, Electrochemical properties of novel ionic liquids for electric double layer capacitor applications, *Electrochim. Acta* 49 (2004) 3603–3611.
- H. Xing, C. Liao, Q. Yang, G.M. Veith, B. Guo, X.G. Sun, Q. Ren, Y.S. Hu, S. Dai, Ambient lithium-SO<sub>2</sub> batteries with ionic liquids as electrolytes, *Angew. Chem. Int. Ed.* 53 (2014) 2099–2103.
- M. Armand, F. Endres, D.R. MacFarlane, H. Ohno, B. Scrosati, Ionic-liquid materials for the electrochemical challenges of the future, *Nat. Mater.* 8 (2009) 621–629.
- M. Ishikawa, T. Sugimoto, M. Kikuta, E. Ishiko, M. Kono, Pure ionic liquid electrolytes compatible with a graphitized carbon negative electrode in rechargeable lithium-ion batteries, *J. Power Sources* 162 (2006) 658–662.
- T. Sugimoto, M. Kikuta, E. Ishiko, M. Kono, M. Ishikawa, Ionic liquid electrolytes compatible with graphitized carbon negative with additive and their effects on interfacial properties, *J. Power Sources* 183 (2008) 436–440.
- T. Sugimoto, Y. Atsumi, M. Kikuta, E. Ishiko, M. Kono, M. Ishikawa, Ionic liquid electrolyte systems based on bis(fluorosulfonyl)imide for lithium-ion batteries, *J. Power Sources* 189 (2009) 802–805.
- R. Sheldon, Catalytic reactions in ionic liquids, *Chem. Commun.* (2001) 2399–2407.
- Y. Abe, Y. Yagi, S. Hayase, M. Kawatsura, T. Itoh, Ionic liquid engineering for lipase-mediated optical resolution of secondary alcohols: design of Ionic Liquids Applicable to ionic liquid coated-lipase catalyzed reaction, *Ind. Eng. Chem. Res.* 51 (2012) 9952–9958.
- F. Zhou, Y. Liang, W. Liu, Ionic liquid lubricants: designed chemistry for engineering applications, *Chem. Soc. Rev.* 38 (2009) 2590–2599.
- A. Somers, P. Howlett, D. MacFarlane, M. Forsyth, A review of ionic liquid lubricants, *Lubricants* 1 (2013) 3–21.
- K. Yoshii, K. Yamaji, T. Tsuda, H. Matsumoto, T. Sato, R. Izumi, T. Torimoto, S. Kuwabata, Highly durable Pt nanoparticle-supported carbon catalysts for the oxygen reduction reaction tailored by using an ionic liquid thin layer, *J. Mater. Chem. A* 4 (2016) 12152–12157.
- T. Torimoto, K.-i. Okazaki, T. Kiyama, K. Hirahara, N. Tanaka, S. Kuwabata, Sputter deposition onto ionic liquids: simple and clean synthesis of highly dispersed ultra-fine metal nanoparticles, *Appl. Phys. Lett.* 89 (2006) 243117.
- S. Kuwabata, H. Minamoto, K. Inoue, A. Imanishi, K. Hosoya, H. Uyama, T. Torimoto, T. Tsuda, S. Seki, Three-dimensional micro/nano-scale structure fabricated by combination of non-volatile polymerizable RTIL and FIB irradiation, *Sci Rep* 4 (2014) 3722.
- T. Tsuda, N. Nemoto, K. Kawakami, E. Mochizuki, S. Kishida, T. Tajiri, T. Kushibiki, S. Kuwabata, SEM observation of wet biological specimens pretreated with room-temperature ionic liquid, *ChemBiochem* 12 (2011) 2547–2550.
- T. Tsuda, E. Mochizuki, S. Kishida, H. Sakagami, S. Tachibana, M. Ebisawa, N. Nemoto, Y. Nishimura, S. Kuwabata, Observation of electrochemical reaction and biological specimen by novel analytical technique combined with room-temperature ionic liquid and scanning electron microscope, *Electrochemistry* 80 (2012) 308–311.
- T. Torimoto, T. Tsuda, K. Okazaki, S. Kuwabata, New frontiers in materials science opened by ionic liquids, *Adv. Mater.* 22 (2010) 1196–1221.
- S. Kuwabata, T. Tsuda, T. Torimoto, Room-temperature ionic liquid. A new medium for material production and analyses under vacuum conditions, *J. Phys. Chem. Lett.* 1 (2010) 3177–3188.
- K. Yoshii, K. Yamaji, T. Tsuda, K. Tsunashima, H. Yoshida, M. Ozaki, S. Kuwabata, Physicochemical properties of tri-*n*-butylkxylphosphonium cation-based room-temperature ionic liquids, *J. Phys. Chem. B* 117 (2013) 15051–15059.
- R. Hagiwara, K. Matsumoto, Y. Nakamori, T. Tsuda, Y. Ito, H. Matsumoto, K. Momota, Physicochemical properties of 1,3-dialkylimidazolium fluorohydrogenate room-temperature molten salts, *J. Electrochem. Soc.* 150 (2003) D195–D199.
- T. Tsuda, K. Kondo, M. Baba, S. Suwa, Y. Ikeda, T. Sakamoto, S. Seino, H. Yoshida, M. Ozaki, A. Imanishi, S. Kuwabata, Physicochemical properties of 1-alkyl-3-methylimidazolium chloride–urea melts, *Electrochim. Acta* 100 (2013) 285–292.
- Z.J. Chen, J.M. Lee, Free volume model for the unexpected effect of C2-methylation on the properties of imidazolium ionic liquids, *J. Phys. Chem. B* 118 (2014) 2712–2718.
- Z.J. Chen, H.W. Xi, K.H. Lim, J.M. Lee, Distillable ionic liquids: reversible amide O-alkylation, *Angew. Chem. Int. Ed.* 52 (2013) 13392–13396.
- K. Matsumoto, R. Hagiwara, Y. Ito, Room temperature molten fluorometallates: 1-ethyl-3-methylimidazolium hexafluoroantimonate(V) and hexafluorotantalate(V), *J. Fluor. Chem.* 115 (2002) 133–135.
- J. Sun, M. Forsyth, D.R. MacFarlane, Room-temperature molten salts based on the quaternary ammonium ion, *J. Phys. Chem. B* 102 (1998) 8858–8864.
- Z.-B. Zhou, H. Matsumoto, K. Tatsumi, Cyclic quaternary ammonium ionic liquids with perfluoroalkyltrifluoroborates: synthesis, characterization, and properties, *Chem. Eur. J.* 12 (2006) 2196–2212.
- K. Nakamura, T. Shikata, Systematic dielectric and NMR study of the ionic liquid 1-alkyl-3-methylimidazolium, *ChemPhysChem* 11 (2010) 285–294.
- A. Aupoix, B. Pégot, G. Vo-Thanh, Synthesis of imidazolium and pyridinium-based ionic liquids and application of 1-alkyl-3-methylimidazolium salts as pre-catalysts for the benzoin condensation using solvent-free and microwave activation, *Tetrahedron* 66 (2010) 1352–1356.
- K. Iwasaki, K. Yoshii, S. Tsuzuki, H. Matsumoto, T. Tsuda, S. Kuwabata, Alkali metal salts with designable aryltrifluoroborate anions, *J. Phys. Chem. B* 120 (2016) 9468–9476.
- A.J. Lennox, G.C. Lloyd-Jones, Preparation of organotrifluoroborate salts: precipitation-driven equilibrium under non-etching conditions, *Angew. Chem. Int. Ed.* 51 (2012) 9385–9388.
- J.S. Wilkes, M.J. Zaworotko, Air and water stable 1-ethyl-3-methylimidazolium based ionic liquids, *J. Chem. Soc. Chem. Commun.* 965–967 (1992).
- D. Zhao, Z. Fei, C.A. Ohlin, G. Laurency, P.J. Dyson, Dual-functionalised ionic liquids: synthesis and characterisation of imidazolium salts with a nitrile-functionalised anion, *Chem. Commun.* (2004) 2500–2501.
- Z.-B. Zhou, M. Takeda, M. Ue, New hydrophobic ionic liquids based on perfluoroalkyltrifluoroborate anions, *J. Fluor. Chem.* 125 (2004) 471–476.
- Z.-B. Zhou, H. Matsumoto, K. Tatsumi, Structure and properties of new ionic liquids based on alkyl- and alkenyltrifluoroborates, *ChemPhysChem* 6 (2005) 1324–1332.
- H. Matsumoto, H. Sakaebe, K. Tatsumi, Preparation of room temperature ionic liquids based on aliphatic onium cations and asymmetric amide anions and their electrochemical properties as a lithium battery electrolyte, *J. Power Sources* 146 (2005) 45–50.
- Z.-B. Zhou, H. Matsumoto, K. Tatsumi, Low-melting, low-viscous, hydrophobic ionic liquids: 1-alkyl(alkyl ether)-3-methylimidazolium perfluoroalkyltrifluoroborate, *Chem. Eur. J.* 10 (2004) 6581–6591.
- Z.-B. Zhou, H. Matsumoto, K. Tatsumi, Low-viscous, hydrophobic ionic liquids: aliphatic quaternary ammonium salts with perfluoroalkyltrifluoroborates, *Chem. Eur. J.* 11 (2005) 752–766.
- Z.-B. Zhou, H. Matsumoto, K. Tatsumi, Low-viscous, low-melting, hydrophobic ionic liquids: 1-Alkyl-3-methylimidazolium Trifluoromethyltrifluoroborate, *Chem. Lett.* 33 (2004) 680–681.
- Z.-B. Zhou, H. Matsumoto, K. Tatsumi, A new class of hydrophobic ionic liquids: trialkyl(2-methoxyethyl)ammonium perfluoroethyltrifluoroborate, *Chem. Lett.* 33 (2004) 886–887.
- M.J. Frisch, G.W. Trucks, H.B. Schlegel, G.E. Scuseria, M.A. Robb, J.R. Cheeseman, G. Scalmani, V. Barone, B. Mennucci, G.A. Petersson, H. Nakatsuji, M. Caricato, X. Li, H.P. Hratchian, A.F. Izmaylov, J. Bloino, G. Zheng, J.L. Sonnenberg, M. Hada, M. Ehara, K. Toyota, R. Fukuda, J. Hasegawa, M. Ishida, T. Nakajima, Y. Honda, O. Kitao, H. Nakai, T. Vreven, J.A. Montgomery Jr., J.E. Peralta, F. Ogliaro, M.J. Bearpark, J. Heyd, E.N. Brothers, K.N. Kudin, V.N. Staroverov, R. Kobayashi, J. Normand, K. Raghavachari, A.P. Rendell, J.C. Burant, S.S. Iyengar, J. Tomasi, M. Cossi, N. Rega, N.J. Millam, M. Klene, J.E. Knox, J.B. Cross, V. Bakken, C. Adamo, J. Jaramillo, R. Gomperts, R.E. Stratmann, O. Yazyev, A.J. Austin, R. Cammi, C. Pomelli, J.W. Ochterski, R.L. Martin, K. Morokuma, V.G. Zakrzewski, G.A. Voth, P. Salvador, J.J. Dannenberg, S. Dapprich, A.D. Daniels, Ö. Farkas, J.B. Foresman, J.V. Ortiz, J. Cioslowski, D.J. Fox, Gaussian 09, Gaussian, Inc., Wallingford, CT, 2009.
- P.R. Rablen, J.F. Hartwig, Accurate borane sequential bond dissociation energies by high-level ab initio computational methods, *J. Am. Chem. Soc.* 118 (1996) 4648–4653.
- J.G. Huddleston, A.E. Visser, W.M. Reichert, H.D. Willauer, G.A. Broker, R.D. Rogers, Characterization and comparison of hydrophilic and hydrophobic room temperature ionic liquids incorporating the imidazolium cation, *Green Chem.* 3 (2001) 156–164.
- K. Nishikawa, S. Wang, H. Katayangi, S. Hayashi, H.O. Hamaguchi, Y. Koga, K. Tozaki, Melting and freezing behaviors of prototype ionic liquids, 1-butyl-3-

- methylimidazolium bromide and its chloride, studied by using a nano-watt differential scanning calorimeter, *J. Phys. Chem. B* 111 (2007) 4894–4900.
- [45] Y. Shimizu, K. Fujii, M. Imanari, K. Nishikawa, Phase behavior of a Piperidinium-based room-temperature ionic liquid exhibiting scanning rate dependence, *J. Phys. Chem. B* 119 (2015) 12552–12560.
- [46] H.D.B. Jenkins, H.K. Roobottom, J. Passmore, L. Glasser, Relationships among ionic lattice energies, molecular (formula unit) volumes, and thermochemical radii, *Inorg. Chem.* 38 (1999) 3609–3620.
- [47] I. Krossing, J.M. Slattery, C. Daguinet, P.J. Dyson, A. Oleinikova, H. Weingartner, Why are ionic liquids liquid? A simple explanation based on lattice and solvation energies, *J. Am. Chem. Soc.* 128 (2006) 13427–13434.
- [48] J.M. Slattery, C. Daguinet, P.J. Dyson, T.J. Schubert, I. Krossing, How to predict the physical properties of ionic liquids: a volume-based approach, *Angew. Chem. Int. Ed.* 46 (2007) 5384–5388.
- [49] S. Tsuzuki, Factors controlling the diffusion of ions in ionic liquids, *ChemPhysChem* 13 (2012) 1664–1670.
- [50] H. Tokuda, K. Ishii, M.A. Susan, S. Tsuzuki, K. Hayamizu, M. Watanabe, Physicochemical properties and structures of room-temperature ionic liquids. 3. Variation of cationic structures, *J. Phys. Chem. B* 110 (2006) 2833–2839.
- [51] C.A. Angell, W. Xu, M. Yoshizawa, A. Hayashi, J.-P. Belieres, P. Lucas, M. Videa, Physical chemistry of ionic liquids: inorganic and organic as well as protic and aprotic, in: H. Ohno (Ed.), *Electrochemical Aspects of Ionic Liquids*, John Wiley & Sons, Inc., New Jersey 2005, pp. 5–26.
- [52] C.A. Angell, Free volume model for transport in fused salts: electrical conductance in glass-forming nitrate melts, *J. Phys. Chem.* 68 (1964) 1917–1929.
- [53] C.T. Moynihan, C.A. Angell, Mass transport in ionic melts at low temperatures. Chronopotentiometric diffusion coefficients of silver(I), cadmium(II), and thallium(I) in calcium nitrate tetrahydrate, *J. Phys. Chem.* 74 (1970) 736–737.
- [54] P.-Y. Chen, C.L. Hussey, Electrodeposition of cesium at mercury electrodes in the tri-1-butylmethylammonium bis((trifluoromethyl)sulfonyl)imide room-temperature ionic liquid, *Electrochim. Acta* 49 (2004) 5125–5138.
- [55] N. Nishi, A. Hashimoto, E. Minami, T. Sakka, Electrocapillarity and zero-frequency differential capacitance at the interface between mercury and ionic liquids measured using the pendant drop method, *Phys. Chem. Chem. Phys.* 17 (2015) 5219–5226.
- [56] H. Tokuda, K. Hayamizu, K. Ishii, M.A.B.H. Susan, M. Watanabe, Physicochemical properties and structures of room temperature ionic liquids. 1. Variation of anionic species, *J. Phys. Chem. B* 108 (2004) 16593–16600.
- [57] W. Xu, E.I. Cooper, C.A. Angell, Ionic liquids: ion mobilities, glass temperatures, and fragilities, *J. Phys. Chem. B* 107 (2003) 6170–6178.
- [58] H. Matsumoto, Electrochemical windows of room-temperature ionic liquids, in: H. Ohno (Ed.), *Electrochemical Aspects of Ionic Liquids*, John Wiley & Sons, Inc., New Jersey 2005, pp. 35–54.
- [59] C.L. Hussey, The electrochemistry of room-temperature haloaluminate molten salts, in: G. Mamantov, A.I. Popov (Eds.), *Chemistry of Nonaqueous Solutions*, VCH Publishers, New York 1994, pp. 227–275.